Nonlocal effects on the spontaneous emission near a plasmonic nanowire

Paola Góngora-Lugo and Jesús A. Maytorena*
Centro de Nanociencias y Nanotecnología, Universidad Nacional Autónoma de México, Apartado Postal 2681, 22800 Ensenada, Baja California, Mexico
(Received 30 August 2016; published 9 June 2017)

We calculate the radiative, nonradiative, and plasmonic decay rates of an individual optical emitter near a metallic nanowire with a nonlocal dielectric response. The potential inside the cylindrical wire is obtained within the random-phase approximation, which allows the nonlocal treatment of the electronic response. The induced field at the site of the emitter is also found. Calculations are carried out using a hydrodynamic dielectric function and the effects introduced by spatial dispersion through surface plasmons and reflection amplitudes are discussed. Nonlocal corrections to the emission rates become more relevant for nanowires with radii in the range of a few nanometers, at exciting frequencies close to the resonances of surface modes, and when the distance between the source dipole and the wire edge is comparable to the wire radius or lies in the subnanometer scale.

DOI: 10.1103/PhysRevA.95.063811

I. INTRODUCTION

The spatial nonlocality of the dielectric response means that the induced polarization at a given position $\mathbf{r}$ depends not only on the exciting electric field at the same point $\mathbf{r}$ but also on the excitation at nearby points $\mathbf{r}'$ [1]. Intrinsic surface effects on dispersion relations, additional plasmon branches, the anomalous skin effect, and surface sensitive contributions to optical spectroscopies, among others, have been recognized as manifestations of nonlocal behavior [1,2]. On the theoretical side, the inclusion of spatial dispersion has to be accounted for in order to achieve a precise comparison between theory and experimental observations.

The advent of plasmonic nanostructures and the increasing versatility and control in nanofabrication techniques have inevitably prompted the investigation of the role of nonlocal effects on the optical properties of such subwavelength systems [3–5]. Dimers of metallic nanoparticles [6–9], narrow gaps between metals with density profiles [10,11], ultrathin films [10], and more complex geometries [12–14] are some examples revealing the effects of spatial nonlocality within a few nanometer distances, sizes, and separations or at a subnanometer scale. Reduction of field enhancement and limitation of confinement, modified shifts of resonances, and new spectral features are typical consequences. At the same time, numerical implementations that take into account the nonlocal character of the dynamical response have been developed, usually based on the phenomenological hydrodynamic model.

Given the characteristic strong confinement and large bandwidth of electromagnetic fields in metallic nanostructures [15], the surface plasmon polaritons have been proposed as an alternative way to achieve strong coherent coupling between individual emitters and evanescent fields [16,17]. In close analogy to cavity QED, this enhanced interaction would be a consequence of the small volume mode associated with the evanescent plasmon field. On the experimental side, this type of coupling was observed in a system of quantum dots near a silver nanowire [18]. These studies have since motivated a number of explorations involving single quantum emitters (atoms, quantum dots, molecules, and qubits) interacting with photons at the nanoscale. Potential applications including quantum information science, sensors, light-emitting diodes, thermal radiation, and nanolasers, among others, are currently being explored [19,20]. Localized plasmon resonances of nanospheres and nanoshells are usually invoked to explore nonlocal effects on the coupling with individual emitters. Some examples are the dramatic reduction of the enhancement of molecular fluorescence [21], the diminution and spectral modification of the Förster energy transfer between two molecules [22], and the substantial discrepancy between the local and nonlocal spectra of the local optical density of states (which is proportional to atomic spontaneous emission rate) as a function of the probe-to-surface separation [23].

The purpose of the present paper is to introduce spatial dispersion in the theory of Chang *et al.* [17] on the spontaneous emission of a dipole located near a plasmonic nanowire. To this end we use the random-phase approximation (RPA) approach developed by Girard and co-workers [24,25] for small metal spherical particles, but adapted to the cylindrical symmetry. Boustimi *et al.* [26] applied it to study the van der Waals interaction between an atom and a nanowire. We will follow the cylindrical eigenmode treatment implemented in [26], but taking a real frequency and a wire with complex dielectric function immersed in a lossless positive dielectric. This self-consistent approach allows us to introduce corrections in the expressions for the emission rates due to coupling with radiative modes, nonradiative losses, and surface plasmons, which take into account spatial nonlocality of the electronic response. The theory of Chang *et al.* uses a local description of the metal response, which will become invalid for small radii and if the dipole is within a few angstroms or nanometers from the wire. For the metal wire, the hydrodynamic dielectric function will be used. This is one of the simplest nonlocal models for the electronic response of a metal [27]. As is well known, in the presence of nonlocality, the induced charge density at the metal surface is smeared out over a screening length. The frequency-dependent position $d_\perp(\omega)$ of its centroid, measured from the nominal surface of the metal, indicates whether the electric potential extends over a region with lower (outside the metal) or higher (inside the metal) average density. A lower (higher) density implies a lower

*jesusm@cnyn.unam.mx

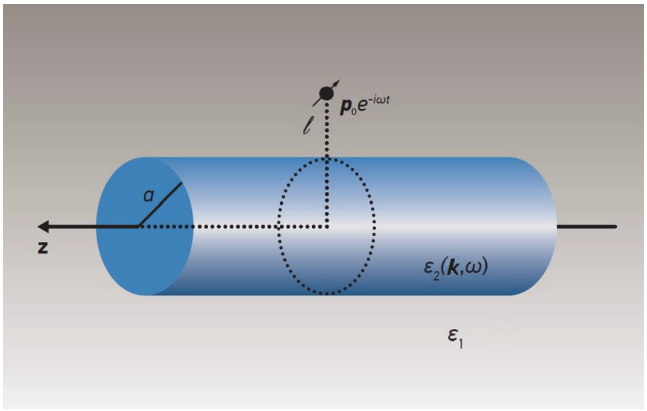

FIG. 1. Oscillating point dipole in the vicinity of a metallic nanowire of radius a with a nonlocal dielectric response $\epsilon_2(\mathbf{k},\omega)$.

(higher) plasmon energy [2]. As a consequence, the dispersion relation of surface plasmons, reflection amplitudes, absorption via electron-hole excitations, and other properties can be significantly modified. Within the hydrodynamic model, we find here that the spontaneous emission can also be notably altered with respect to the local description results.

The paper is organized as follows. In Sec. II we present the expressions for the self-consistent nonlocal potential inside the cylinder and the amplitudes of potentials everywhere in space, as obtained from the RPA approach employed in Ref. [26]. Details of the derivation are presented in the Appendices. The dielectric function of the wire is that of the hydrodynamic model. In particular, we focus on the coefficients giving the potential reflected on the wire surface. In Sec. III we follow the approach of Chang *et al.* [17] and write expressions for the emission rates due to radiative, nonradiative, and plasmonic channels, including spatial dispersion effects that enter through the nonlocal corrections to the reflection coefficients. Our results are discussed in Sec. IV and we summarize in Sec. V.

II. NONLOCAL RESPONSE

We consider the inhomogeneous problem defined by an oscillating point dipole $\mathbf{p} = \mathbf{p}_0 e^{-i\omega t}$ located in the proximity of an infinitely long metallic cylinder of radius a, which is oriented along the z axis and imbedded in a lossless medium with dielectric constant $\epsilon_1 > 1$ (Fig. 1). The distance $d = a + \ell$ between the dipole and the center of the wire is restricted to be much smaller than the wavelength of light, so retardation can be neglected [17,28].

The dipole can lose energy through several channels and the corresponding spontaneous emission rates require the evaluation of potentials and fields. As we mentioned above, we will follow Ref. [26]. Thus we just display the main expressions and leave some derivational steps for the Appendices.

To obtain the charges and potentials induced by the dipole source, we will consider first the problem of a single point charge and then apply the operator $\mathbf{p}_0 \cdot \nabla'$ to derive the expressions corresponding to the dipole. All charge and field quantities have a common harmonic time dependence, which we omit for simplicity.

Outside the cylinder (region 1), the potential is $\Phi_1(\mathbf{r}) = \Phi_0(\mathbf{r}) + \Phi_r(\mathbf{r})$, where Φ_0 is the potential produced by a unit point charge located at $\mathbf{r}' = (\rho' > a, \varphi', z')$ and Φ_r is the potential due to the charge induced in the wire. The usual cylindrical representation of the electrostatic free-space Green's function allows us to write, for $\rho < \rho'$,

$$\Phi_0(\mathbf{r},\mathbf{r}') = \frac{1}{\epsilon_1}\sum_{n=-\infty}^{\infty}\int_{-\infty}^{\infty} dk_\parallel A_n(k_\parallel,\rho',\varphi',z') I_n(k_\parallel\rho) e^{in\varphi} e^{ik_\parallel z}, \tag{1}$$

where $K_n(x)$ and $I_n(x)$ are the modified Bessel functions and $A_n(k_\parallel,\rho',\varphi',z') = K_n(k_\parallel\rho') e^{-in\varphi'} e^{-ik_\parallel z'}/\pi$. The reflected potential, which satisfies $\nabla^2\Phi_r = 0$, can be expanded in a similar fashion:

$$\Phi_r(\mathbf{r},\mathbf{r}') = \sum_{n=-\infty}^{\infty}\int_{-\infty}^{\infty} dk_\parallel A_n(k_\parallel,\rho',\varphi',z') K_n(k_\parallel\rho) a_n(k_\parallel) e^{in\varphi} e^{ik_\parallel z}. \tag{2}$$

Following [26], the effective or self-consistently screened potential inside the cylinder (region 2) can be written in the form (see Appendix A)

$$\Phi_2(\mathbf{r},\mathbf{r}',\omega) = \sum_{n=-\infty}^{\infty}\int_{-\infty}^{\infty} dk_\parallel A_n(k_\parallel,\rho',\varphi',z') F_n(k_\parallel,\rho,\omega) b_n(k_\parallel) e^{in\varphi} e^{ik_\parallel z}, \tag{3}$$

where

$$F_n(k_\parallel,\rho,\omega) = a\sum_{k_\perp}\sum_{k'_\perp} B_n(k_\perp) B_n(k'_\perp) J_n(k'_\perp a) J_n(k_\perp\rho) E_n^{-1}(k_\parallel,k_\perp,k'_\perp,\omega), \tag{4}$$

$B_n(k_\perp)$ is a normalization factor, $J_n(x)$ is the Bessel function of integer order, and $k_\perp$ is the radial wave-vector component. The function $E_n/(k_\parallel^2 + k_\perp^2)$ is the RPA dielectric constant appropriate for this problem [26]. Thus, the function F_n contains all the nonlocal and dynamical information of the metal wire.

At this point, the continuity of potentials and fields at $\rho = a$ allows us to find the coefficients $a_n(k_\parallel)$ and $b_n(k_\parallel)$,

$$a_n(k_\parallel,\omega) = -\frac{1}{\epsilon_1}\frac{I_n(k_\parallel a) - \epsilon_1 k_\parallel F_n(k_\parallel,a,\omega) I_n'(k_\parallel a)}{K_n(k_\parallel a) - \epsilon_1 k_\parallel F_n(k_\parallel,a,\omega) K_n'(k_\parallel a)}, \quad (5)$$

$$b_n(k_\parallel,\omega) = k_\parallel \frac{K_n(k_\parallel a) I_n'(k_\parallel a) - K_n'(k_\parallel a) I_n(k_\parallel a)}{K_n(k_\parallel a) - \epsilon_1 k_\parallel F_n(k_\parallel,a,\omega) K_n'(k_\parallel a)}. \quad (6)$$

When $\epsilon_1 = 1$, the expression (5) reduces to that reported in [26].

To evaluate $F_n(k_\parallel,\rho,\omega)$ in (4), we first assume a homogeneous dielectric response of the free-electron metal, which implies $E_n(k_\parallel,k_\perp,k_\perp',\omega) = E_n(\mathbf{k},\omega)\delta_{k_\perp',k_\perp} = k^2\epsilon(\mathbf{k},\omega)\delta_{k_\perp',k_\perp}$, where $\epsilon(\mathbf{k},\omega)$ is the nonlocal bulk dielectric function of the metal (see Appendix A). When the nonlocal response of the free electrons in the metal is neglected, this function reduces to a scalar $E_n(k_\parallel,k_\perp,k_\perp',\omega) = (k_\parallel^2 + k_\perp^2)\epsilon(\omega)\delta_{k_\perp',k_\perp}$, where $\epsilon(\omega)$ is the local dielectric function. The function F_n [Eq. (4)] simplifies then to

$$F_n(k_\parallel,\rho,\omega) = a\sum_{k_\perp} \frac{B_n^2(k_\perp) J_n(k_\perp a) J_n(k_\perp \rho)}{k^2\epsilon(\mathbf{k},\omega)}. \quad (7)$$

To describe the spatial dispersion [1] effects, we use the hydrodynamic model [27] to express the longitudinal dielectric constant of the cylinder

$$\epsilon(\mathbf{k},\omega) = 1 - \frac{\omega_p^2}{\omega(\omega + i\gamma) - \beta^2(k_\parallel^2 + k_\perp^2)}, \quad (8)$$

where ω_p is the plasma frequency, γ^{-1} is a phenomenological relaxation time, $\beta^2 = v_F^2/3$ is the spatial dispersion parameter accounting for the pressure gradient of a free-electron gas, and v_F is the Fermi velocity.

The discrete sum in (7) can be evaluated analytically by a procedure very similar to that employed in the eigenmode treatment of the nonlocal response of small spheres [29] (see Appendix B). The result is

$$F_n(k_\parallel,\rho,\omega) = \frac{1}{\epsilon_2(\omega)}\frac{I_n(k_\parallel\rho)}{k_\parallel I_n'(k_\parallel a)} + \left(\frac{\epsilon_2(\omega) - 1}{\epsilon_2(\omega)}\right)\frac{I_n(\kappa\rho)}{\kappa I_n'(\kappa a)}, \quad (9)$$

where

$$\kappa^2 = k_\parallel^2 - \frac{\omega(\omega + i\gamma) - \omega_p^2}{\beta^2} \quad (10)$$

and $\epsilon_2(\omega) = 1 - \omega_p^2/\omega(\omega + i\gamma)$. In the local limit $\beta \to 0$, $I_n(y)/yI_n'(y) \to 0$, and F_n reduces to the first term in (9). Using this $F_n^{\rm loc}(k_\parallel,a,\omega)$ in (5), (6), (2), and (3), the same local results reported in Ref. [17] are obtained. The factor (9) allows us to write (5) as

$$a_n(k_\parallel) = -\frac{1}{\epsilon_1}\frac{(\epsilon_2 - \epsilon_1) I_n(k_\parallel a) I_n'(k_\parallel a) - \epsilon_1(\epsilon_2 - 1)\eta_n(\kappa a) k_\parallel a I_n'^2(k_\parallel a)}{\epsilon_2 K_n(k_\parallel a) I_n'(k_\parallel a) - \epsilon_1 K_n'(k_\parallel a) I_n(k_\parallel a) - \epsilon_1(\epsilon_2 - 1)\eta_n(\kappa a) k_\parallel a K_n'(k_\parallel a) I_n'(k_\parallel a)}, \quad (11)$$

where

$$\eta_n(\kappa a) = \frac{1}{\kappa a}\frac{I_n(\kappa a)}{I_n'(\kappa a)} \quad (12)$$

is the factor accounting for the nonlocal corrections to the reflections coefficients within the hydrodynamic model.

We will need the expressions in the limit $k_\parallel a \ll 1$. For $n = 0$,

$$a_0 \approx -\frac{1}{\epsilon_1}\frac{\epsilon_2 - \epsilon_1 - \epsilon_1(\epsilon_2 - 1)k_\parallel^2\eta_0(\kappa a)/2}{\epsilon_1[2(k_\parallel a)^{-2} - \eta_0(\kappa a)] - \epsilon_2[\ln(k_\parallel a/2) + \gamma_e - \epsilon_1\eta_0(\kappa a)]}, \quad (13)$$

where $\gamma_e = 0.5772\ldots$ is the Euler constant. For $n \neq 0$,

$$a_n \approx -\frac{1}{\epsilon_1}\frac{2}{(n-1)!n!}\left(\frac{k_\parallel^2 a^2}{4}\right)^n g_n(\kappa a,\omega), \quad (14)$$

where

$$g_n(\kappa a,\omega) = \frac{\epsilon_2(\omega) - \epsilon_1[1 + n(\epsilon_2(\omega) - 1)\eta_n(\kappa a)]}{\epsilon_2(\omega) + \epsilon_1[1 + n(\epsilon_2(\omega) - 1)\eta_n(\kappa a)]}. \quad (15)$$

When $\eta_n \to 0$ (local limit), $g_n(\kappa a,\omega) \to r_p^0(\omega) = [\epsilon_2(\omega) - \epsilon_1]/[\epsilon_2(\omega) + \epsilon_1]$, which coincides with the nonretarded limit of the reflection amplitude for p-polarized light of a plane metallic surface [2].

The vanishing of the denominator of the coefficient a_n [Eq. (5)], for some value of $k_\parallel$, means that a finite response can be obtained from an infinitesimal excitation, i.e., the system may oscillate spontaneously, only when the reflection coefficient a_n has a pole. The condition for this resonance is written as $K_n(k_\parallel a) = \epsilon_1 k_\parallel K_n'(k_\parallel a) F_n(k_\parallel,a,\omega)$, or from (11),

$$\frac{1}{1 - \epsilon_2(\omega)/\epsilon_1} = k_\parallel a\, I_n'(k_\parallel a) K_n(k_\parallel a)\left[1 - \epsilon_1\left(\frac{\epsilon_2(\omega) - 1}{\epsilon_2(\omega) - \epsilon_1}\right)\frac{k_\parallel a K_n'(k_\parallel a)}{K_n(k_\parallel a)}\eta_n(\kappa a)\right]. \quad (16)$$

The roots of this transcendental equation provide the dispersion relation of the plasmons, including both surface and volume plasmons; when $\epsilon_1 = 1$ and for real $\epsilon_2(\omega)$ ($\gamma = 0$) the expression reduces to that obtained in [30]. The modes given

by the dispersion relation (16) are consistent with those of a careful implementation of the quasistatic approximation [5].

In the limit $k_\parallel a \ll 1$, the dispersion relation for the axially symmetric mode $n = 0$ is given by [see (13)]

$$\frac{\epsilon_2(\omega)}{\epsilon_1} = \frac{1}{(k_\parallel a)^2}\frac{2-(k_\parallel a)^2\eta_0(\kappa a)}{\ln(k_\parallel a/2)+\gamma_e-\epsilon_1\eta_0(\kappa a)} \tag{17}$$

and for the higher-order modes $n \neq 0$ [see (14)],

$$\epsilon_2(\omega)+\epsilon_1 = -n\epsilon_1[\epsilon_2(\omega)-1]\eta_n(\kappa a). \tag{18}$$

The higher-order resonances present nonzero cutoff frequencies [30], which in the local limit all converge to the same frequency, to the solution of $\epsilon_2(\omega) = -\epsilon_1$, as in a flat surface. Equation (18) resembles the electrostatic dispersion relation of the surface plasmon of a plane surface [2]. This suggests that the quantity $a\eta_n(\kappa a)$ can be interpreted as an effective screening length at the cylindrical surface.

III. DECAY RATES

Within a local treatment, expressions for radiative, nonradiative, and plasmonic contributions to the total spontaneous emission rate of a dipole close to a nanowire have been derived by Klimov and Ducloy [28] and Chang *et al.* [17]. In our case, the corrections due to spatial dispersion enter through the reflection coefficients (11) and therefore the corresponding expressions for the decay rates can be obtained along the same lines. Here we just sketch the steps and present the final expressions, emphasizing the differences with respect to the local results.

A. Radiative channel

The radiative decay accounts for the energy radiated to the far zone. Far away from the source, there would be a dipolar contribution due to the source and reflected potentials, $\Phi_{\rm dip} = (\mathbf{p}_0\cdot\nabla')(\Phi_0+\Phi_r)$. Given that the radiative decay rate is proportional to the radiation power, the normalized radiative spontaneous decay rate can be written as [28,31]

$$\frac{\Gamma_{\rm rad}}{\Gamma_0} = \frac{|\mathbf{p}_0+\delta\mathbf{p}|^2}{|\mathbf{p}_0|^2}, \tag{19}$$

where $\delta\mathbf{p}$ is the induced dipole moment in the cylinder, $\Gamma_0 = \sqrt{\epsilon_1}|\mathbf{p}_0|^2k_0^3/3\hbar$ is the decay rate of an excited dipole in free space, and $k_0 = \omega/c$. The induced dipole can be determined from the reflected potential $\Phi_{{\rm dip},r} = (\mathbf{p}_0\cdot\nabla')\Phi_r$ by extracting a contribution having the form $\delta\Phi = \delta\mathbf{p}\cdot\mathbf{r}/r^3$. If $\delta\mathbf{p} = \delta p_\rho\hat{\boldsymbol{\rho}}' + \delta p_\varphi\hat{\boldsymbol{\varphi}}' + \delta p_z\hat{\mathbf{z}}$, we look for a contribution in $\Phi_{{\rm dip},r}$ of the form

$$\delta\Phi = \delta p_\rho\frac{\rho\cos(\varphi-\varphi')}{(\rho^2+z^2)^{3/2}} + \delta p_\varphi\frac{\rho\sin(\varphi-\varphi')}{(\rho^2+z^2)^{3/2}} + \delta p_z\frac{z}{(\rho^2+z^2)^{3/2}}.$$

It can be seen from (2) that only the terms with $n = \pm1$ are responsible for this contribution,

$$\begin{aligned}\Phi_r^{|n|=1}(\mathbf{r},\mathbf{r}') &= \Phi_r^{n=-1}+\Phi_r^{n=+1}\\ &= \frac{2}{\pi}\cos(\varphi-\varphi')\\ &\quad\times\int_{-\infty}^{\infty}dk_\parallel K_1(k_\parallel\rho)K_1(k_\parallel\rho')a_1(k_\parallel)e^{ik_\parallel(z-z')}\\ &\approx -\frac{1}{\epsilon_1}g_1(\kappa_0a,\omega)\frac{a^2}{\rho'}\frac{\rho\cos(\varphi-\varphi')}{[\rho^2+(z-z')^2]^{3/2}},\end{aligned} \tag{20}$$

where the last line has been obtained after noting that for large ρ, the main contribution to the integral comes from a small region around $k_\parallel\rho \approx 1$, which allows the replacement of $K_1(k_\parallel\rho')$ and $a_1(k_\parallel)$ by their expansions around $k_\parallel = 0$ [see (14)] and to leading order in $k_\parallel$. Here $g_1(\kappa_0a,\omega)$ is obtained from (15), with $\kappa_0^2 = [\omega_p^2-\omega(\omega+i\gamma)]/\beta^2$ [see (10)].

Choosing the parameters $\rho' = d$ and $z' = 0$ and keeping only terms $\sim 1/r^3 = (\rho^2+z^2)^{3/2}$, the corresponding dipolelike contribution $\delta\Phi$ is given by $\Phi_{{\rm dip},r}^{|n|=1}(\mathbf{r},\mathbf{r}') = (\mathbf{p}_0\cdot\nabla')\Phi_r^{|n|=1}(\mathbf{r},\mathbf{r}')$, with $\delta p_\rho = p_{0,\rho}g_1(\kappa_0a,\omega)a^2/d^2$, $\delta p_\varphi = -p_{0,\varphi}g_1(\kappa_0a,\omega)a^2/d^2$, and $\delta p_z = 0$. Thus, for a dipole pointing along each direction, the corresponding radiative decay (19) is given by

$$\left(\frac{\Gamma_{\rm rad}}{\Gamma_0}\right)_\rho = \left|1+g_1(\Omega,u)\frac{a^2}{d^2}\right|^2, \tag{21}$$

$$\left(\frac{\Gamma_{\rm rad}}{\Gamma_0}\right)_\varphi = \left|1-g_1(\Omega,u)\frac{a^2}{d^2}\right|^2, \tag{22}$$

$$\left(\frac{\Gamma_{\rm rad}}{\Gamma_0}\right)_z = 1, \tag{23}$$

where we have rewritten the reflection factor $g_1(\kappa_0a,\omega)$ as $g_1(\Omega,u)$, given that $(\kappa_0a)^2 = u^2[1-\Omega(\Omega+i\tilde{\gamma})]$, with $\Omega = \omega/\omega_p$, $\tilde{\gamma} = \gamma/\omega_p$, and $u = a\omega_p/\beta$ which is the parameter of spatial nonlocality [30]. The local limit corresponds to $u\to\infty$, $g_1(\Omega,u\to\infty) = r_p^0(\omega)$, as was noted previously.

B. Nonradiative channel

The nonradiative decay rate of the oscillating dipole is due to losses inside the cylinder and it can be obtained from the dissipated power $\mathcal{P} = \frac{\omega}{2}{\rm Im}\,[\mathbf{p}_0\cdot\mathbf{E}_{\rm loc}]$, where $\mathbf{E}_{\rm loc}$ is the field acting at the position of the dipole after being scattered by the cylinder [31]. Thus, we have, for the rate $\Gamma_{\rm nonrad} = \mathcal{P}/\hbar\omega$,

$$\begin{aligned}\frac{\Gamma_{\rm nonrad}}{\Gamma_0} &= \frac{3}{2\sqrt{\epsilon_1}k_0^3}{\rm Im}\left[\frac{\mathbf{p}_0\cdot\mathbf{E}_r(\mathbf{r}',\mathbf{r}')}{|\mathbf{p}_0|^2}\right]\\ &= -\frac{3}{2\sqrt{\epsilon_1}k_0^3}{\rm Im}\left[\frac{\mathbf{p}_0}{|\mathbf{p}_0|^2}\cdot\nabla(\mathbf{p}_0\cdot\nabla')\Phi_r(\mathbf{r},\mathbf{r}')\Big|_{\mathbf{r}=\mathbf{r}'}\right].\end{aligned}$$

For each orientation of the exciting dipole, this expression leads to [28]

$$\left(\frac{\Gamma_{\rm nonrad}}{\Gamma_0}\right)_\rho = -\frac{3}{\pi k_0^3\sqrt{\epsilon_1}}\sum_{n=0}^{\infty}(2-\delta_{n,0})\int_0^\infty dk_\parallel k_\parallel^2[K_n'(k_\parallel d)]^2{\rm Im}[a_n(k_\parallel)] \tag{24}$$

for $\mathbf{p}_0 = p_{0,\rho}\hat{\boldsymbol{\rho}}'$,

$$\left(\frac{\Gamma_{\rm nonrad}}{\Gamma_0}\right)_\varphi = -\frac{6}{\pi k_0^3\sqrt{\epsilon_1}}\sum_{n=0}^{\infty}\frac{n^2}{d^2}\int_0^\infty dk_\parallel [K_n(k_\parallel d)]^2 {\rm Im}[a_n(k_\parallel)] \tag{25}$$

for $\mathbf{p}_0 = p_{0,\varphi}\hat{\boldsymbol{\varphi}}'$, and

$$\left(\frac{\Gamma_{\rm nonrad}}{\Gamma_0}\right)_z = -\frac{3}{\pi k_0^3\sqrt{\epsilon_1}}\sum_{n=0}^{\infty}(2-\delta_{n,0})\int_0^\infty dk_\parallel k_\parallel^2 [K_n(k_\parallel d)]^2 {\rm Im}[a_n(k_\parallel)] \tag{26}$$

for $\mathbf{p}_0 = p_{0,z}\hat{\mathbf{z}}$. Following Chang *et al.* [17], we will exclude the term $n = 0$ in the evaluation of these sums in order to consider separately the pole contribution from the factor a_0, which corresponds to the excitation of the fundamental plasmon mode.

C. Plasmonic channel

It is well known that the $n = 0$ plasmon field becomes strongly localized on a scale $\sim a$ around the metal surface for radius well below the diffraction limit. The small volume associated with this mode suggests that it can interact strongly with nearby emitters. The decay rate into this localized plasmon is obtained from the expression

$$\left(\frac{\Gamma_{pl}}{\Gamma_0}\right)_\rho = -\frac{3}{\pi k_0^3\sqrt{\epsilon_1}}{\rm Im}\left[\int_0^\infty dk_\parallel k_\parallel^2 K_1^2(k_\parallel d)a_0(k_\parallel)\right]_{\rm pole} \tag{27}$$

in the absence of losses, for the case of a radially oriented dipole. From (11), the reflection coefficient $a_0(x)$ is given by $a_0(x) = -N_0(x)/\epsilon_1 D_0(x)$, where the numerator N_0 is

$$N_0(x) = (\epsilon_2-\epsilon_1)I_0(x)I_1(x) - \epsilon_1(\epsilon_2-1)\eta_0(\kappa a)x I_1^2(x) \tag{28}$$

and the denominator D_0 is

$$\begin{aligned} D_0(x) = {}& \epsilon_2 K_0(x)I_1(x) + \epsilon_1 K_1(x)I_0(x) \\ & + \epsilon_1(\epsilon_2-1)\eta_0(\kappa a)x K_1(x)I_1(x), \end{aligned} \tag{29}$$

with $x = k_\parallel a$. The pole satisfies $D_0(\tilde{x}) = 0$, with $\tilde{x} = \tilde{k}_\parallel a = C$. In the vicinity of this pole, $D_0(x) \approx (x-\tilde{x})D_0'(\tilde{x})$ and

$$a_0(x) \approx -\frac{1}{\epsilon_1}\frac{N_0(x)}{(x-\tilde{x})D_0'(\tilde{x})},$$

where

$$\begin{aligned} D_0'(x) = {}& (\epsilon_2-\epsilon_1)[K_0(x)I_0(x) - K_1(x)I_1(x)] \\ & - \frac{1}{x}[\epsilon_2 K_0(x)I_1(x) + \epsilon_1 K_1(x)I_0(x)] \\ & + \epsilon_1(\epsilon_2-1)\Big[\eta_0(\kappa a)\{x[K_1(x)I_0(x) - K_0(x)I_1(x)] \\ & - K_1(x)I_1(x)\} + x K_1(x)I_1(x)\frac{d\eta_0(\kappa a)}{dx}\Big], \end{aligned} \tag{30}$$

with

$$\frac{d\eta_0(\kappa a)}{dx} = \frac{x}{(\kappa a)^2}\left[1 - \left(\frac{I_0(\kappa a)}{I_1(\kappa a)}\right)^2\right].$$

Substitution into the integral (27) leads to

$$\left(\frac{\Gamma_{pl}}{\Gamma_0}\right)_\rho = \alpha_{pl}\frac{K_1^2(Cd/a)}{(k_0 a)^3}, \tag{31}$$

with

$$\alpha_{pl} = \frac{6}{\epsilon_1^{3/2}}\frac{C^2 N_0(C)}{D_0'(C)}. \tag{32}$$

Similarly,

$$\left(\frac{\Gamma_{pl}}{\Gamma_0}\right)_\varphi = 0, \quad \left(\frac{\Gamma_{pl}}{\Gamma_0}\right)_z = \alpha_{pl}\frac{K_0^2(Cd/a)}{(k_0 a)^3}. \tag{33}$$

In these expressions the nonlocal factor $\eta_0(\kappa a)$ becomes $\eta_0(\tilde{\kappa}a)$, where $(\tilde{\kappa}a)^2 = (\tilde{k}_\parallel a)^2 - (\omega^2-\omega_p^2)a^2/\beta^2 = C^2 + u^2(1-\Omega^2)$. Although they have the same form as for the local case, in the presence of spatial dispersion ($\beta \neq 0$) the values of a_0 and therefore of the roots C become modified as can be seen from (17), the last term in N_0 (28), and the last line of (30).

IV. RESULTS

In the following we show results for a sodium nanowire [4] embedded in a medium with dielectric constant $\epsilon_1 = 2$. The parameters are $\hbar\omega_p = 6.04$ eV, $\gamma/\omega_p = 0.026$, and $v_F/c = 3.5\times10^{-3}$. The parameter of nonlocality is then given by $u = a\times 15\ {\rm nm}^{-1}$, which hints that the radius should be of a few nanometers in order to have appreciable spatial dispersion effects. We will consider two wire radii $a = 1$ nm ($u = 15$) and $a = 5$ nm ($u = 75$).

We first consider the radiative contributions (21) and (22) to the spontaneous decay rate, which we recast as

$$\begin{aligned} \left(\frac{\Gamma_{\rm rad}}{\Gamma_0}\right)_\rho = {}& 1 + |g_1(\Omega,u)|^2\frac{a^4}{(a+\ell)^4} \\ & + 2\,{\rm Re}[g_1(\Omega,u)]\frac{a^2}{(a+\ell)^2}, \end{aligned} \tag{34}$$

$$\begin{aligned} \left(\frac{\Gamma_{\rm rad}}{\Gamma_0}\right)_\varphi = {}& 1 + |g_1(\Omega,u)|^2\frac{a^4}{(a+\ell)^4} \\ & - 2\,{\rm Re}[g_1(\Omega,u)]\frac{a^2}{(a+\ell)^2}, \end{aligned} \tag{35}$$

where $\ell = d - a$ is the distance between the dipole and the wire edge. Within a local description, this radiative contribution is determined by the reflection amplitude r_p^0 of a *flat* surface. However, when the curvature $1/a$ increases

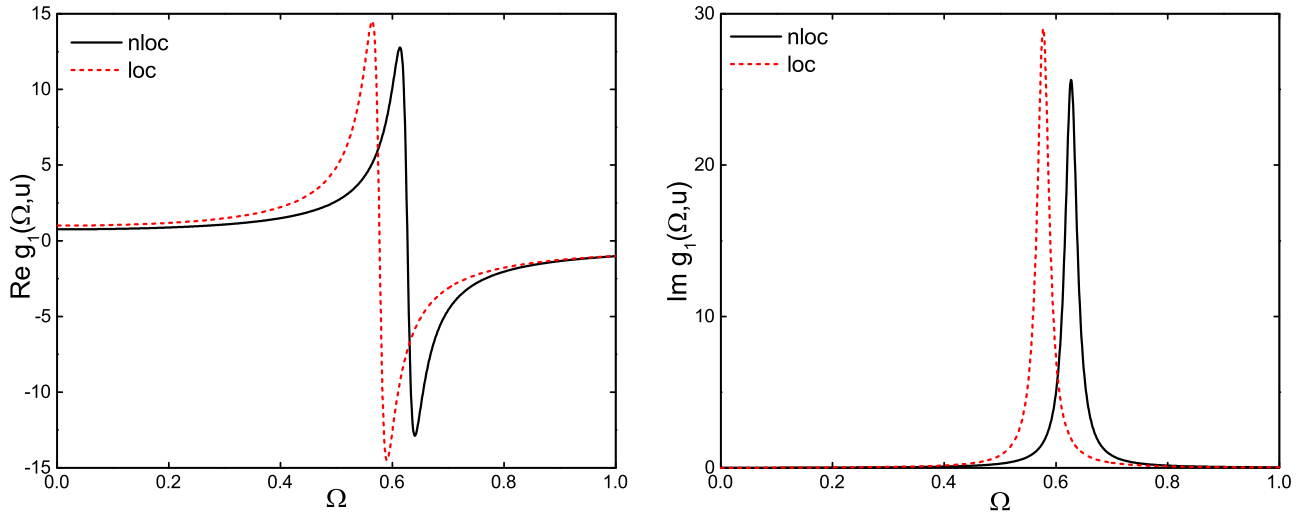

FIG. 2. Real (left) and imaginary (right) parts of the nonlocal reflection factor $g_1(\Omega,u)$, which determines the induced dipole in a sodium wire of radius $a = 1$ nm ($u = 15$). The local result corresponds to $g_1(\Omega,u \to \infty)$.

enough, spatial dispersion has to be accounted for. Nonlocal hydrodynamic effects are expected to be important mostly in a surface region of width $1/\kappa_0 \sim \beta/\omega_p$ (for frequencies well below ω_p). Thus, for small $\kappa_0 a \sim a\omega_p/\beta$ and for dipoles close to the screening region, the more significant nonlocal corrections in $\Gamma_{\rm rad}/\Gamma_0$ should appear.

In Fig. 2 we show the nonlocal reflection amplitude $g_1(\Omega,u)$ for a wire radius $a = 1$ nm ($u = 15$), in comparison to the nondispersive ($u \to \infty$) Fresnel amplitude $r_p^0(\Omega)$. The blueshift of the resonance is associated with the presence of spatial dispersion. It is well known that within the hydrodynamic model of a flat metal surface with an abrupt density profile, the screening charge density occupies a finite region inside the surface, having a centroid given by $d_\perp(\omega) = \kappa_0^{-1} = [(\omega_p^2 - \omega^2)/\beta^2]^{-1/2}$, and the induced potential extends over a region of higher density. This means that most of the screening takes place within the metal. By analogy, in the case of a cylinder, the centroid would be $d_\perp(\omega) = \{\kappa_0[I_1'(\kappa_0 a)/I_1(\kappa_0 a)]\}^{-1}$. Thus we can think of the wire as having effectively a lesser radius and therefore supporting a surface resonance with higher energy [Eq. (18)].

Figure 3 plots local and nonlocal $(\Gamma_{\rm rad}/\Gamma_0)_\rho$ as a function of the separation ℓ, for two values of the wire radius, $a = 1$ and 5 nm. We investigate this function by varying Ω across the resonance of the response function $g_1(\Omega,u)$. Results are shown for four different frequencies: (i) top left, $\Omega < \Omega_{sp}$, well below the poles of $g_1(\Omega,u = 15)$ and $g_1(\Omega,u \to \infty) = r_p^0(\omega)$, located at $\Omega^* = 0.62$ and $\Omega_{sp} = 1/\sqrt{\epsilon_1 + 1} = 0.57$, respectively; (ii) top right, $\Omega \approx \Omega_{sp}$; (iii) bottom left, $\Omega \approx \Omega^*$; and (iv) bottom right, $\Omega > \Omega^*$, well above any resonance.

At $\Omega = 0.20$, it is found that the values of the decay rate obtained within the nonlocal description are smaller than those from the local theory, for the range of dipole-wire separation ℓ shown. This is because, at this frequency, the spatial dispersion modifications to the reflection factors are such that $\mathrm{Re}(r_p^0) > \mathrm{Re}(g_1) > 0$ [see Eq. (21) or (34)]. We also note that $(\Gamma_{\rm rad}/\Gamma_0)_\rho$ is larger for increasing wire radius for a given ℓ, although the contrast between local and nonlocal results is more appreciable for decreasing radius and for closer dipoles. As the wire becomes thinner, the decay rate drops faster as a function of ℓ and clear deviations from local theory start at $\ell \lesssim a$. Qualitatively similar behavior can be seen at $\Omega = 0.50$. However, given that this frequency is closer to the local resonance in r_p^0 while still separated from that of g_1, the magnitude of $(\Gamma_{\rm rad}/\Gamma_0)_\rho$ is clearly enhanced and the difference between the local and nonlocal results increases, particularly for separations $\ell < a$. In contrast, at $\Omega = 0.65$, lying closer to the pole of g_1 instead of the local resonance, $(\Gamma_{\rm rad}/\Gamma_0)_\rho$ is further enhanced and can take values above the local results. For $a = 1$ nm it is strongly enhanced when ℓ is within few angstroms and diminishes rapidly again as a function of ℓ, with respect to the local result and also compared to the $a = 5$ nm case. Given that both $\mathrm{Re}(g_1)$ and $\mathrm{Re}(r_p^0)$ become negative at this frequency, the decay rate curve develops a minimum at some ℓ for each radius, as shown in the inset. On the other hand, a dramatic change of the overall shape of $\Gamma_{\rm rad}(\ell)$ occurs at $\Omega = 0.80$, away from any resonance. At this exciting frequency, $\mathrm{Re}(g_1) < \mathrm{Re}(r_p^0) < 0$ and Eq. (34) implies that now $(\Gamma_{\rm rad}/\Gamma_0)_\rho < 1$, which can exhibit a minimum for some value of the distance ℓ. Again, the local and nonlocal results are very close, the differences being larger for the thinner wire when the dipole is located at $\ell \lesssim a$.

The case of a dipole emitter pointing azimuthally is shown in Fig. 4. Note that Eq. (22) differs only by a minus sign from Eq. (21). This suggests that the results can be understood qualitatively from the radial case with the change $g_1 \to -g_1$. For instance, at $\Omega = 0.20$, $\mathrm{Re}(-r_p^0) < \mathrm{Re}(-g_1) < 0$ and the results look similar to those of the radial case at $\Omega = 0.80$ where both the local and nonlocal reflection factors are also negative, with $\mathrm{Re}(g_1) < \mathrm{Re}(r_p^0) < 0$. The rate $(\Gamma_{\rm rad}/\Gamma_0)_\varphi$ vs ℓ is then greater than that of the local model, each curve exhibits a minimum, grows faster to unity for decreasing radius, and decreases for increasing radius. On the other hand, the rate $(\Gamma_{\rm rad}/\Gamma_0)_\varphi$ at $\Omega = 0.80$ resembles $(\Gamma_{\rm rad}/\Gamma_0)_\rho$ at $\Omega = 0.20$ for similar reasons, given that now $\mathrm{Re}(-g_1) > \mathrm{Re}(-r_p^0) > 0$ like before $\mathrm{Re}(r_p^0) > \mathrm{Re}(g_1) > 0$. In the proximity of Ω_{sp} (Fig. 4, top right) or Ω^* (Fig. 4, bottom left), the rate $(\Gamma_{\rm rad}/\Gamma_0)_\varphi$ can be explained along the same lines. At distances smaller than $\ell \sim a$

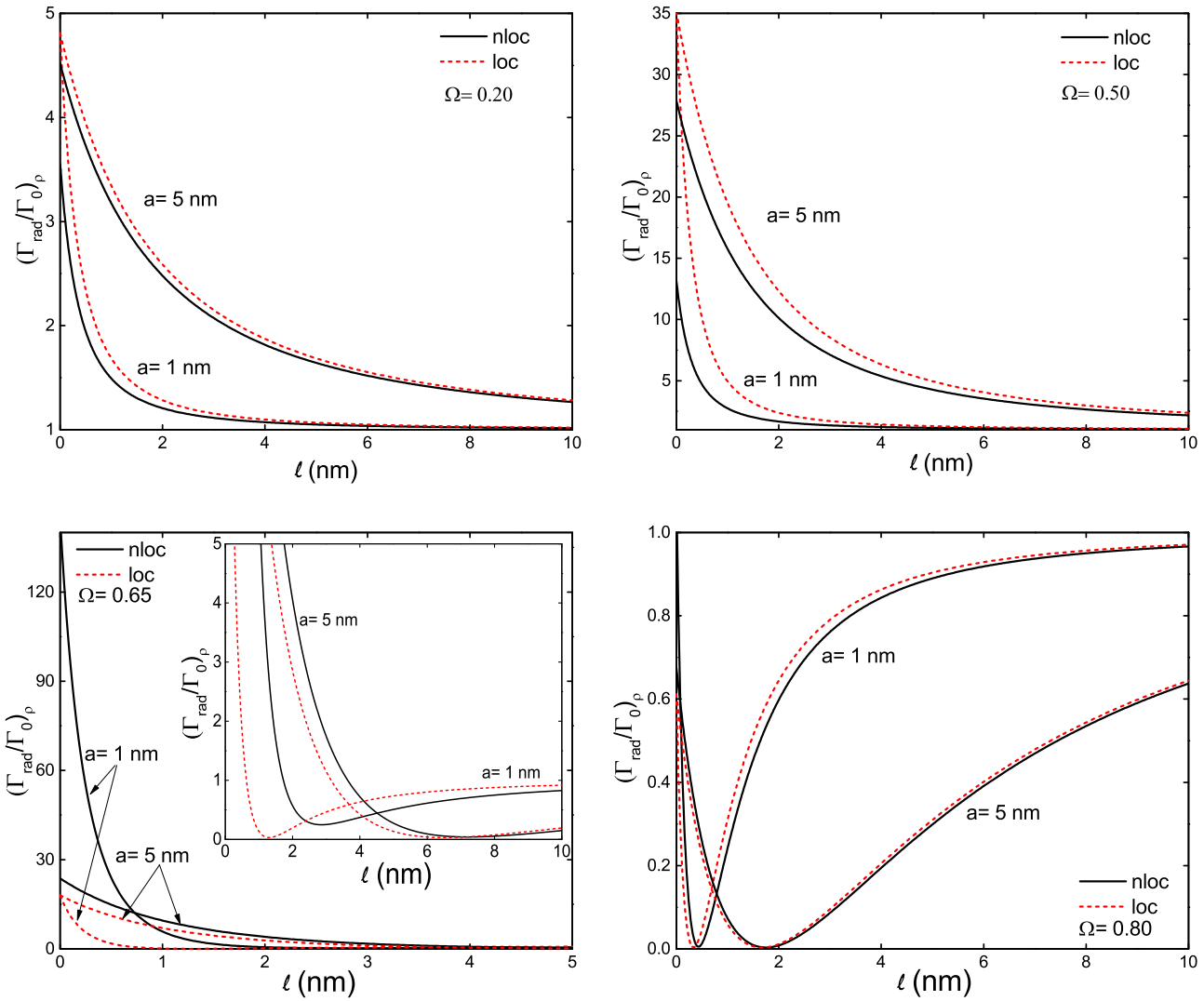

FIG. 3. Local and nonlocal spontaneous radiative decay rate as a function of the distance $\ell = d - a$ between a radially oriented dipole and the edge of a Na nanowire, for frequencies $\Omega = \omega/\omega_p$ well below (top left), close to (top right and bottom left), and well above (bottom right) the pole of the nonlocal response function $g_1(\Omega, u = 15)$, located at $\Omega^* = 0.62$. For $a = 1$ nm, the parameter of nonlocality is $u = a\omega_p/\beta = 15$.

the rate is enhanced but the spatial dispersion reduces notably its magnitude with respect to that within the nondispersive model.

As a function of frequency, $\Gamma_{\rm rad}/\Gamma_0$ has a dependence determined by the reflection factor $g_1(\Omega, u)$. Thus, the local and nonlocal rates present the same spectral features, but with the latter blueshifted. It turns out, however, that at their respective resonances, the nonlocal values $\Gamma_{\rm rad}(\ell, \Omega = \Omega^*)$ are clearly below those of the local calculation $\Gamma_{\rm rad}(\ell, \Omega = \Omega_{sp})$, for $\ell, a \lesssim 2$ nm.

We now turn on the decay rate into the $n = 0$ surface plasmon of the wire. Within a Fermi golden rule approach [17], $\Gamma_{pl} = 2\pi g^2(\mathbf{r}, \omega) D(\omega)$, where $g^2(\mathbf{r}, \omega) \sim K_1^2(Cd/a)/a^2$ is the position-dependent emitter-field coupling strength and $D(\omega) \sim (d\omega/dk_\parallel)^{-1}$ is the density of states of surface plasmons. As is well known, the fundamental surface mode of a nanowire is strongly localized due to a large wave vector $k_\parallel \sim 1/a$ and its (local) dispersion relation reveals that the group velocity $v_g \sim \omega a$ is drastically reduced and the density of states is enhanced. This fact, in addition to the small effective mode area, leads to a strong coupling between the dipole and the surface plasmons of the nanowire.

On the other hand, in the presence of spatial nonlocality, the dispersion relation of the surface mode shows that the density of states decreases with respect to the local case, notably for increasing frequencies and decreasing radius. Thus, one could anticipate that this fact will contribute to the reduction of Γ_{pl}/Γ_0 when compared to the local result. Moreover, as a function of the wire-dipole distance for fixed a and Ω, the plasmonic decay rate within the local vs nonlocal comparison will depend on the balance between $\alpha_{pl}^{\rm loc}(C_{\rm loc}) K_1^2(C_{\rm loc} d/a)$ and $\alpha_{pl}^{\rm nloc}(C_{\rm nloc}) K_1^2(C_{\rm nloc} d/a)$ [Eq. (31)]. This is illustrated in Fig. 5, where we show $(\Gamma_{pl}/\Gamma_0)_\rho(\ell)$ for two frequencies and $a = 1$ nm. We concentrate on separation ℓ within a few nanometers, where the highest values arise and where the contrast between the local and nonlocal results is more important. The inset in the left panel displays the dispersion relation of the fundamental surface plasmon of the wire for $u = 15$, 75, and ∞. It can be noted that $C_{\rm loc} > C_{\rm nloc}$, which implies $K_1^2(C_{\rm loc} d/a) < K_1^2(C_{\rm nloc} d/a)$ (for $a = 1$ nm,

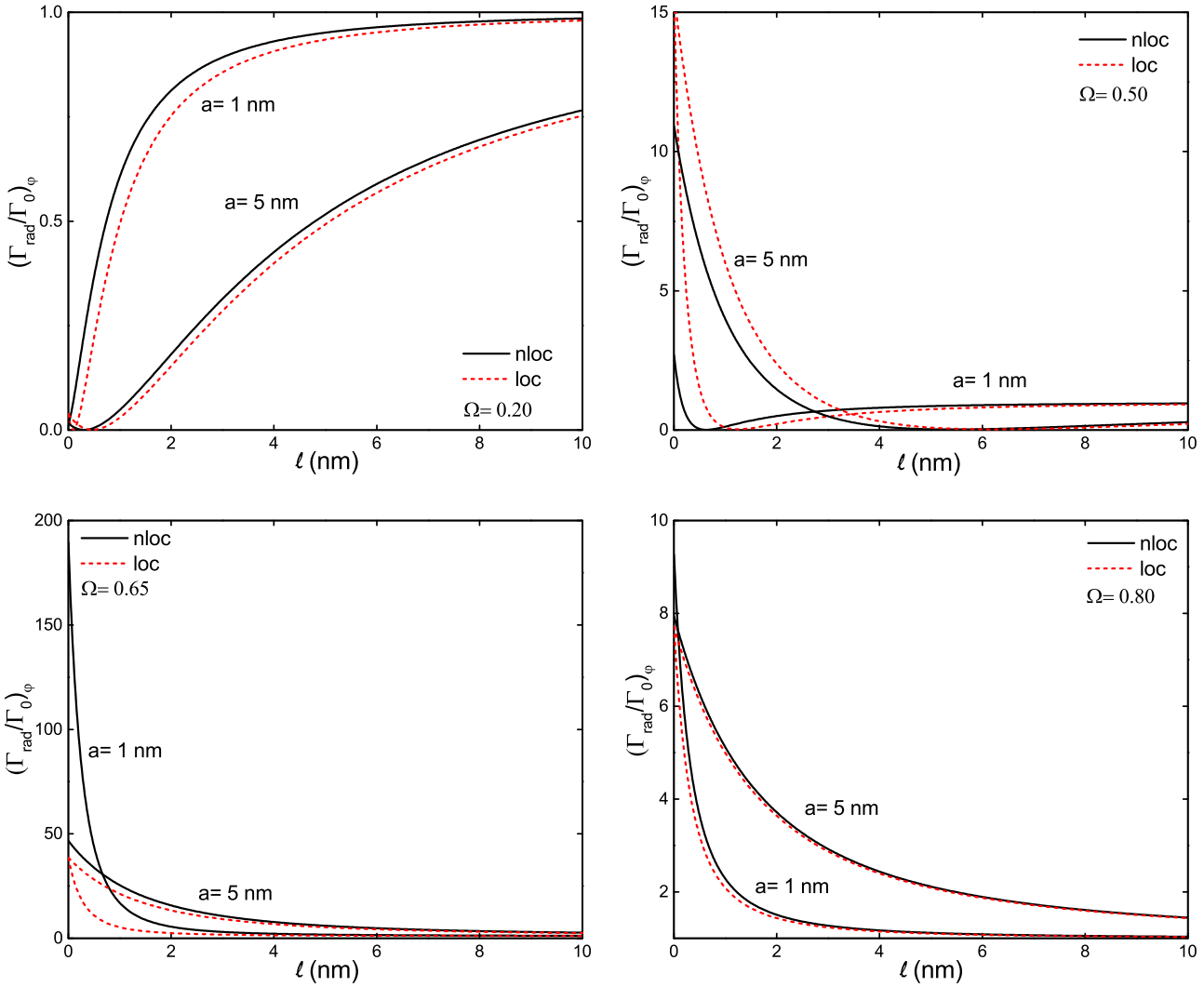

FIG. 4. Radiative decay rate, as in Fig. 1, but for a dipole pointing in the azimuthal direction.

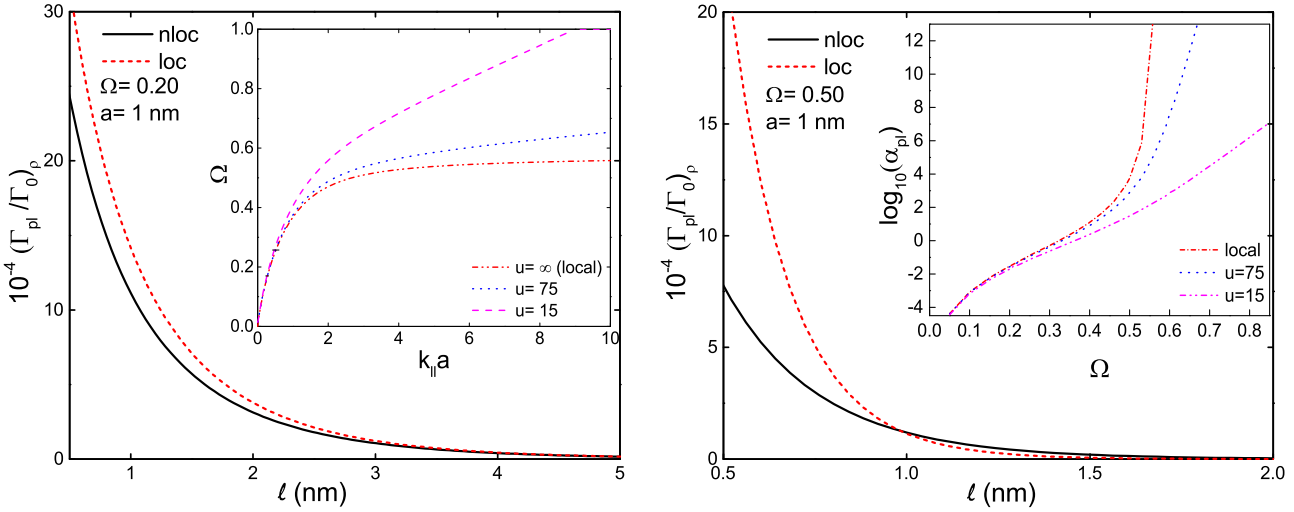

FIG. 5. Spontaneous emission rate into the fundamental surface plasmon of a Na nanowire, as a function of the distance between a radial dipole and the wire edge, shown on the left for low frequency $\Omega = 0.20$, with the inset showing the local ($u = \infty$) and nonlocal dispersion relations of the surface mode for $a = 1$ nm ($u = 15$) and 5 nm ($u = 75$), and on the right for high frequency $\Omega = 0.50$, close to the local electrostatic resonance $\Omega_{sp} = 0.57$, with the inset showing the coefficient α_{pl} of the plasmonic decay rate.

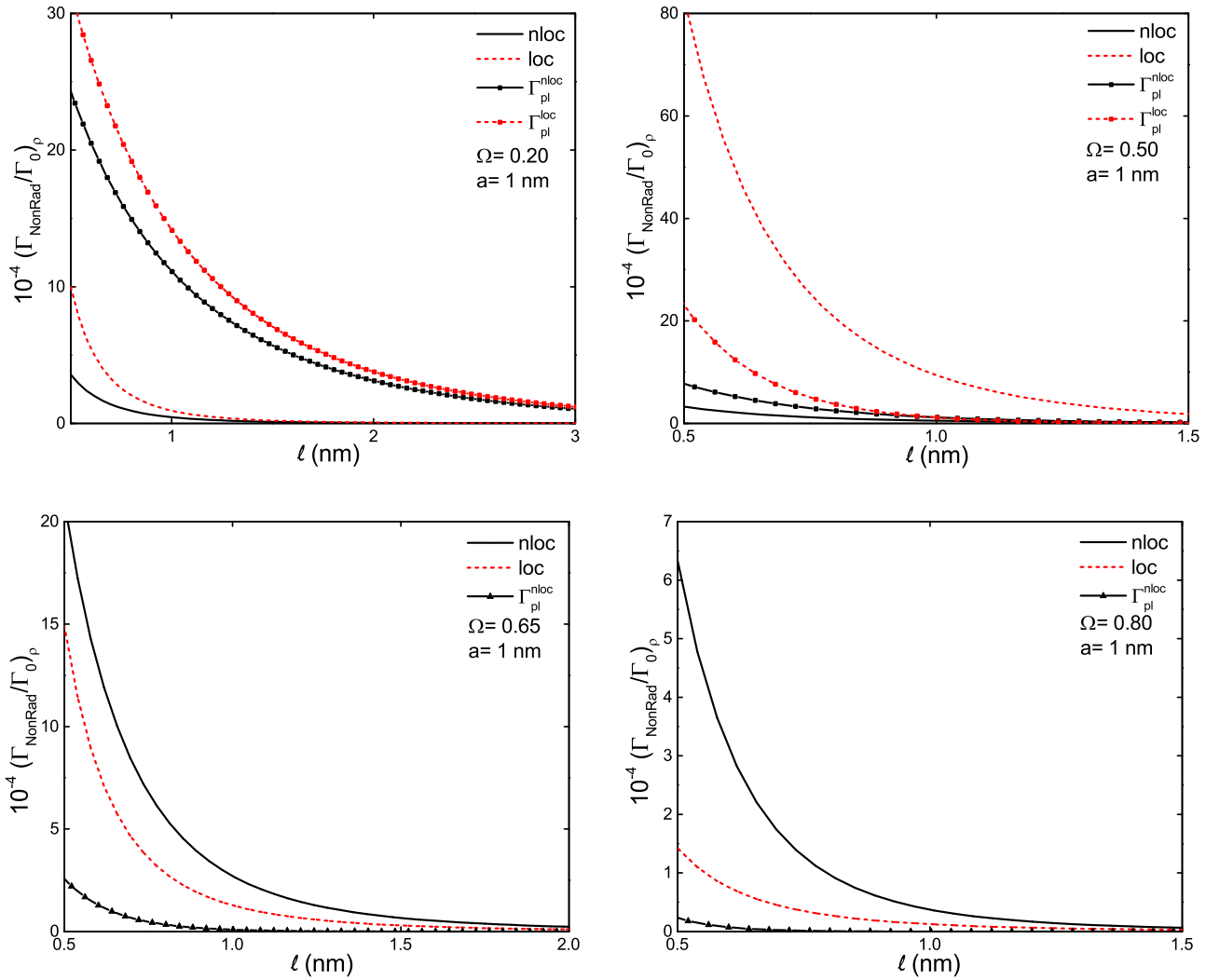

FIG. 6. Nonradiative emission rate of a radial dipole as a function of its distance to a sodium nanowire.

$C_{\rm loc} = 0.36$ and $C_{\rm nloc} = 0.33$ at $\Omega = 0.20$, and $C_{\rm loc} = 2.67$ and $C_{\rm nloc} = 1.53$ at $\Omega = 0.50$). However, as a result, we find $\alpha_{pl}^{\rm loc}(C_{\rm loc}) > \alpha_{pl}^{\rm nloc}(C_{\rm nloc})$, as can be seen in the inset in the right panel. This causes the plasmonic decay rate obtained from the nonlocal theory to be smaller than that of the local theory. The difference between the local and nonlocal calculations, relative to the local value, is about 20–25 % at $\Omega = 0.20$ for $0.5\ {\rm nm} < \ell < 1\ {\rm nm}$. At $\Omega = 0.50$ the main difference takes place for smaller values of ℓ; it is ≈63% for $\ell = 0.5$ nm. We note that for this frequency, the roots $C_{\rm loc}$ and $C_{\rm nloc}$ increase and also its difference. Therefore, smaller values of ℓ will be needed to compensate for the drop of $K_1^2(Cd/a)$. There is a global decrease of the magnitude of the local and nonlocal $\Gamma_{pl}(\ell)$, but the difference between them increases, due to the relative values of the coefficients α_{pl} at this frequency (see the inset in the right panel). However, for frequencies close enough to Ω_{sp}, the corresponding values of $C_{\rm loc}$ become very large and the difference $C_{\rm loc} - C_{\rm nloc}$ further increases, leading to such small values of $K_1^2(C_{\rm loc}d/a)$ as to compensate for the growing factor $\alpha_{pl}(C_{\rm loc})$. As a consequence, now the overall size of the function $\Gamma_{pl}^{\rm loc}(\ell)$ is reduced and lies below $\Gamma_{pl}^{\rm nloc}(\ell)$. At even higher frequencies, beyond the local resonance Ω_{sp}, $C_{\rm nloc}$ gradually increases, K_1^2 decay faster, and the rate $\Gamma_{pl}^{\rm nloc}(\ell)$ maintains its global drop tendency, despite the increasing values of $\alpha_{pl}^{\rm nloc}$.

We have also found that $\Gamma_{pl}(\Omega)$ decreases monotonically for moderate frequencies, for ℓ and $a \sim 1$ nm, with the local values clearly above the nonlocal ones. However, when the frequency is close to the local electrostatic limit, the strong reduction of the group velocity of the fundamental local mode (left inset in Fig. 5) leads to a drastic decay of the plasmonic rate. The opposite situation can then occur, where $\Gamma_{pl}^{\rm loc}(\Omega) < \Gamma_{pl}^{\rm nloc}(\Omega)$, given the characteristics of the nonlocal dispersion curves.

The behavior of $(\Gamma_{pl}/\Gamma_0)_z(\ell)$ for a dipole pointing along the z direction (not shown) is qualitatively similar, with the overall magnitude slightly reduced, due to the presence of the factor $K_0^2 < K_1^2$. Again, nonlocal effects on the emission rate into plasmons are significant for small wire radii and dipoles located at $\ell \sim a$ or at subnanometer distances. The difference (positive or negative) between the local and nonlocal results depends strongly on the frequency.

As for the nonradiative emission rate, we display in Fig. 6 $(\Gamma_{\rm nonrad}/\Gamma_0)_\rho(\ell)$ as obtained from Eq. (24), excluding the

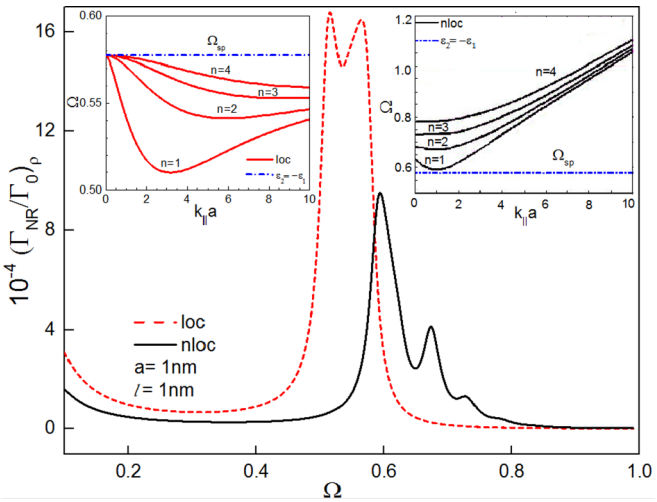

FIG. 7. Nonradiative decay rate vs frequency Ω, for a radial dipole at $\ell = 1$ nm from the edge of a Na nanowire with radius $a = 1$ nm. The insets show the dispersion relation of higher-order ($n \neq 0$) surface modes (left, local; right, nonlocal), characterized by nonzero cutoff frequencies.

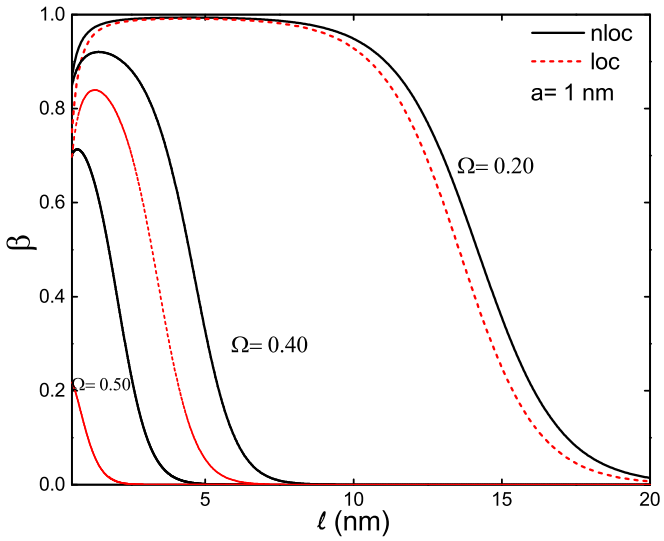

FIG. 8. Spontaneous emission efficiency factor β for a radial dipole, as a function of its distance to the surface of a sodium nanowire.

$n = 0$ term in the sum. We include in the figure the coupling rate into the fundamental surface plasmon ($n = 0$). The observed behavior is mainly controlled by the reflection factors $a_n(k_\parallel)$ involved in the first terms in the sum (24). For a given Ω, the pole structure of $\mathrm{Im}\, a_n(k_\parallel)$ for each $n \neq 0$ determines the magnitude of the nonradiating coupling rate. Again, for frequencies close to Ω_{sp} or below, the spatial dispersion reduces the decay rate $\Gamma^{\mathrm{nloc}}_{\mathrm{nonrad}}(\ell) < \Gamma^{\mathrm{loc}}_{\mathrm{nonrad}}(\ell) < \Gamma_{pl}(\ell)$ for $\ell \lesssim a$. The plasmonic contribution (local or nonlocal) lies clearly above the nonradiative one. At $\Omega = 0.50$, however, the local nonradiative rate becomes greater than the rest because of the proximity to the local resonance, where only $\mathrm{Im}\, a^{\mathrm{loc}}_n(k_\parallel)$ with $n = 1$ presents a resonant contribution. A sharper contrast between the local and nonlocal nonradiative rate is clearly visible. At $\Omega \lesssim \Omega_{sp}$, $\Gamma^{\mathrm{nloc}}_{\mathrm{nonrad}}(\ell) < \Gamma_{pl}(\ell) < \Gamma^{\mathrm{loc}}_{\mathrm{nonrad}}(\ell)$. On the other hand, an opposite situation arises at $\Omega = 0.65$, where only $\mathrm{Im}\, a^{\mathrm{nloc}}_1(k_\parallel)$ displays a resonant behavior: The overall size of nonradiative coupling in the dispersive case increases above all, $\Gamma^{\mathrm{nloc}}_{\mathrm{nonrad}}(\ell) > \Gamma^{\mathrm{loc}}_{\mathrm{nonrad}}(\ell) > \Gamma^{\mathrm{nloc}}_{pl}(\ell)$. At higher frequencies, the resonant nature of terms with $n > 1$ enters, but with smaller amplitude, leading to rates with smaller overall magnitude. For other dipole orientations, the results are qualitatively similar, slightly smaller in size.

Figure 7 shows $(\Gamma_{\mathrm{nonrad}}/\Gamma_0)_\rho$ as a function of the relative frequency for $\ell = 1$ nm and $a = 1$ nm. In contrast to the decay rate through the radiative channel, we note that the spectrum of the nonradiative rate in the nonlocal theory displays not only a blueshift when compared to the local result, but also well-separated peaks. As shown in the right inset, the dispersion curves of higher-order ($n \neq 0$) surface modes [30][1] lie above the local electrostatic resonance of a flat surface Ω_{sp} [solution of $\epsilon_2(\Omega) = -\epsilon_1$] and present nonzero cutoff frequencies [Eq. (18)]. The first peak at $\Omega = 0.59$ arises mainly from the contribution associated with the pole structure of $\mathrm{Im}a_1(k_\parallel)$ in the sum (24), the second peak at $\Omega = 0.67$ comes from the poles in $\mathrm{Im}a_2(k_\parallel)$, the third peak at $\Omega = 0.72$ is due to $\mathrm{Im}a_3(k_\parallel)$, and so on. In contrast, the local dispersion curves (left inset) all lie below Ω_{sp} in a narrower interval of frequencies. As a consequence, the local spectrum consists of two main features only. The first peak at $\Omega = 0.51$ originates from the resonant structure of $\mathrm{Im}a_1(k_\parallel)$, which involves a small interval of $k_\parallel$ around the minimum of the $n = 1$ local dispersion relation. The wider structure around $\Omega = 0.56$ involves all the functions $\mathrm{Im}a_n(k_\parallel)$ in (24), the larger contributions coming from the $n = 2,3,4$ terms.

In Fig. 8 we show the factor $\beta(\ell) = \Gamma_{pl}/\Gamma_{\mathrm{tot}}$ for $\ell =$ 0.5–20 nm. This ratio quantifies the coupling efficiency into the surface plasmons of the nanowire relative to the total decay rate $\Gamma_{\mathrm{tot}} = \Gamma_{\mathrm{rad}} + \Gamma_{\mathrm{nonrad}} + \Gamma_{pl}$. The emission rates just discussed are combined to give a function $\beta(\ell)$ whose values in the nonlocal model are greater than those of the local model. The plasmonic rate Γ_{pl} takes the higher values at low frequencies, with a magnitude lying clearly above the radiative and nonradiative contributions. This implies a large value of the β factor. The difference between the local and nonlocal values comes from the respective values of the plasmonic contribution. When the frequency increases ($\Omega = 0.40, 0.50$) the magnitude of the plasmonic rates decreases while the local nonradiative contribution remains larger than the rest. This is reflected in the diminution of the local and nonlocal β factors. At higher frequencies, above Ω_{sp} where there is no more local fundamental plasmon resonance to excite, the ratio $\Gamma^{\mathrm{nloc}}_{\mathrm{nonrad}}(\ell)/\Gamma^{\mathrm{nloc}}_{pl}$ increases, implying further decreasing of β^{nloc}.

At low frequency ($\Omega = 0.20$), $\beta^{\mathrm{nloc}}(\ell)$ and $\beta^{\mathrm{loc}}(\ell)$ are comparable and reach almost 99% each, for a distance about $\ell \approx 4.4$ nm. When the frequency increases, the overall magnitude of the factor clearly decreases and the maximum

[1] In the notation of Ref. [30], the dispersion curves of these surfaces modes are written as $\omega_{m0}(k)$ (first column in Fig. 12 therein). The fundamental mode is ω_{00}.

shifts toward lower distances. At $\Omega = 0.40$, $\beta^{\rm nloc}_{\rm max} \approx 92\%$ and $\beta^{\rm loc}_{\rm max} \approx 84\%$ at $\ell = 1.4$ and 1.3 nm, respectively. At $\Omega = 0.50$, approaching the local surface resonance at Ω_{sp}, $\beta^{\rm nloc}_{\rm max} \approx 71\%$ at $\ell = 0.7$ nm, but $\beta^{\rm loc}$ reduces more drastically to 22% at $\ell = 0.5$ nm. When Ω further increases across the nonlocal resonances, the $\beta^{\rm nloc}$ factor decreases to very small values. Remarkably, in the presence of nonlocality the coupling of the emitter with the fundamental surface plasmon of the wire is still efficient, as a consequence of the characteristic frequency dependence of the emission rate contributions.

Calculations have been presented for the case of a simple metal, such as sodium, but this approach could also be applied to noble metals by just introducing a background permittivity in the dielectric function (8), which models interband transitions or core polarization contributions [1,2,8,10,13]. As a result, we have found that the differences between the local and nonlocal calculations of the decay rates become increasingly important when the radius a and separation ℓ are $\lesssim$1–2 nm. Although the self-consistent method used to include spatial dispersion partially accounts for quantum mechanical effects (quantum electronic pressure), potentially important effects derived from the atomistic nature of the wire should be additionally taken into account for subnanometer sizes. As is the case for many reported implementations of nonlocality in metallic nanostructures [3,5,8,10,12–14], this aspect, related to the discrete nature of the metal, clearly lies beyond the semiclassical method we have used. One possible quantum approach is to employ the time-dependent density-functional theory within the local-density approximation (TDLDA)[2]. One might expect that deformation of wave functions in the spill-out region of the density profile and contributions to the short-range potential at the metal surface arising from electrostatic and exchange-correlation interactions would modify the surface electromagnetic field and correspondingly the decay rates. An alternative framework recently proposed to incorporate quantum effects is the generalized theory of the nonlocal optical response of plasmonic nanostructures [3]. In a hydrodynamiclike approach, the effect of diffusion of induced charges has been incorporated in addition to the quantum electronic pressure. This theory captures size-dependent damping of surface plasmons in small spherical particles (radius 2–6 nm) and reproduces the TDLDA absorption spectra of nanowire (radius ∼5 nm) dimers with subnanometer gap, without invoking quantum tunneling and showing that charge diffusion can be a dominant mechanism behind the nonlocal optical response [3]. It would be very interesting to apply this generalized theory to further explore nonlocal effects on the spontaneous emission of an individual emitter close to a plasmonic nanowire.

V. CONCLUSION

In this paper we have followed a self-consistent approach to include spatial dispersion effects on the spontaneous emission rate of a single dipole source in the proximity of a metallic nanowire with a hydrodynamic dielectric function. We calculated separately nonlocal corrections to the decay rates due to radiative modes, nonradiative losses, and surface plasmons. The radiative channel for spontaneous emission is controlled by the dipolar reflection amplitude $g_1(\Omega,u)$ and depends strongly on the frequency. At low frequencies, well below the resonance of this amplitude, the spatial dispersion slightly reduces the radiative rate function $\Gamma_{\rm rad}(\ell)$, when compared to the local result. However, this changes notably when the frequency is varied across the nonlocal resonance: The nonlocal rate may become of the order of 100% higher with respect to the local calculation, at distances $\ell \sim 1$ nm. The main peak in $\Gamma_{\rm rad}(\Omega)$, due to the long-wavelength surface mode $n = 1$, is blueshifted as compared to the peak in the local model and at resonance $\Gamma^{\rm nloc}_{\rm rad}(\ell,\Omega^*)$ is lower than $\Gamma^{\rm loc}_{\rm rad}(\ell,\Omega_{sp})$ and more so for smaller radii. The nonradiative channel contribution is determined by the absorption factors $\mathrm{Im}\, a_n(k_\parallel)$, $n \geqslant 1$, and presents similar behavior for $\ell \lesssim a$, although about four orders of magnitude larger. As a function of frequency, this contribution displays a spectrum remarkably different from that of the local theory, not only blueshifted but with the magnitude and shape modified, with a series of well-separated peaks related to the characteristics of the nonlocal dispersion curves of the $n \neq 0$ surface modes. The coupling rate into fundamental ($n = 0$), tightly confined, surface plasmons displays a different behavior: The overall size of $\Gamma_{pl}(\ell)$ decreases as frequency varies in the whole range $0 < \Omega < 1$, for $\ell \lesssim a$, with the nonlocal results being larger than the local ones when the frequency approaches the local electrostatic limit. On the other hand, for ℓ and $a \sim 1$ nm, where the nonlocal effects are important, the function $\Gamma_{pl}(\Omega)$ decreases for moderate frequencies, but $\Gamma^{\rm nloc}_{pl}(\Omega)$ can be greater than $\Gamma^{\rm loc}_{pl}(\Omega)$ when the frequency come closer to the local electrostatic limit. The factor $\beta(\ell)$ shows, however, that an efficient coupling between the dipole and the surface plasmons of the nanowire is still possible in the presence of spatial dispersion and that it is manipulable through the frequency dependence of the electronic response.

It is well known that within hydrodynamic model spill-out density effects, electron-hole excitations, and surface local-field effects are among the aspects not included. We hope our work stimulates more realistic theoretical calculations.

ACKNOWLEDGMENT

We acknowledge support from CONACyT-México.

APPENDIX A: NONLOCAL CALCULATION OF THE SELF-CONSISTENT POTENTIAL

To derive a self-consistent expression of the potential Φ_2 inside the cylinder, the first step is to choose a complete basis set of orthogonal functions convenient to the symmetry of the problem, in terms of which any expandable function $f(\mathbf{r})$ can be written. For the cylindrical symmetry, a natural choice [26] is the set of functions $B_n(k_\perp)J_n(k_\perp\rho)e^{in\varphi}e^{ik_\parallel z}$, where n is an integer, $k_{\parallel,\perp}$ are the components of $\mathbf{k} = k_\perp\hat{\boldsymbol{\rho}} + k_\parallel\hat{\mathbf{z}}$, and B_n is a radial normalization factor such that $B_n^2\int_0^a \rho J_n^2(k_\perp\rho)d\rho = 1$. At this point two choices are possible to produce an orthogonal complete set of functions (see [32]). Following [26,29], we choose $[dJ_n(k_\perp\rho)/d\rho]_{\rho=a} = 0$, which implies a discrete spectrum of transverse momentum $k_\perp$. Thus, the coefficients B_n are given by $B_n^{-2}(k_\perp) = (a^2/2)[1-(n^2/k_\perp^2a^2)]J_n^2(k_\perp a)$. Therefore, after a Fourier transform, any electromagnetic quantity $f(\mathbf{r},\omega)$ at a specific frequency ω can be expanded

as

$$f(\rho,\varphi,z;\omega) = \sum_{n=-\infty}^{\infty}\int_{-\infty}^{\infty} dk_\parallel \sum_{k_\perp} B_n(k_\perp) f_n(k_\parallel,k_\perp,\omega) \times J_n(k_\perp\rho)e^{in\varphi}e^{ik_\parallel z} \quad \text{(A1)}$$

with the inverse transformation

$$f_n(k_\parallel,k_\perp,\omega) = \frac{1}{(2\pi)^2} B_n(k_\perp)\int d^3r\, f(\mathbf{r},\omega) \times J_n(k_\perp\rho)e^{-in\varphi}e^{-ik_\parallel z}. \quad \text{(A2)}$$

Accordingly, we write the potential inside the cylinder as

$$\Phi_2(\mathbf{r},\omega) = \sum_{n=-\infty}^{\infty}\int_{-\infty}^{\infty} dk_\parallel \sum_{k_\perp} B_n(k_\perp)\Phi_{2,n}(k_\parallel,k_\perp,\omega) \times J_n(k_\perp\rho)e^{in\varphi}e^{ik_\parallel z}. \quad \text{(A3)}$$

Within the framework of the self-consistent method, the induced charge density $\delta\rho$ is related to the self-consistent field Φ_2 through the nonlocal linear response equation

$$\delta\rho(\mathbf{r},\omega) = \int d^3r'\chi(\mathbf{r},\mathbf{r}',\omega)\Phi_2(\mathbf{r}',\omega), \quad \text{(A4)}$$

where χ is the independent-electron density-density correlation function of the wire. The transformation to the $(k_\parallel,k_\perp,\omega)$ representation (A2) leads to

$$\delta\rho_n(\mathbf{k},\omega) = \sum_{m=-\infty}^{\infty}\int_{-\infty}^{\infty} dk'_\parallel \sum_{k'_\perp} \chi_{nm}(\mathbf{k},\mathbf{k}',\omega)\Phi_{2,m}(k'_\parallel,k'_\perp,\omega), \quad \text{(A5)}$$

where, assuming cylindrical and translational symmetry, $\chi_{nm}(\mathbf{k},\mathbf{k}',\omega) = \chi_n(k_\perp,k'_\perp,\omega)\delta_{nm}\delta(k_\parallel - k'_\parallel)$, with

$$\chi_n(k_\perp,k'_\perp,\omega) = B_n(k_\perp)B_n(k'_\perp)\int d\rho\,\rho J_n(k_\perp\rho) \times \int d\rho'\rho'\chi(\rho,\rho',\omega)J_n(k'_\perp\rho').$$

Equation (A5) reduces to

$$\delta\rho_n(k_\parallel,k_\perp,\omega) = \sum_{k'_\perp}\chi_n(k_\perp,k'_\perp,\omega)\Phi_{2,n}(k_\parallel,k'_\perp,\omega). \quad \text{(A6)}$$

The self-consistency of the problem is obtained after taking into account the electron-electron interaction through the Poisson equation $\nabla^2\Phi_2(\mathbf{r},\omega) = -4\pi\delta\rho(\mathbf{r},\omega)$, which becomes, in the $(\mathbf{k},\omega)$ representation (A2),

$$-4\pi\delta\rho_n(k_\parallel,k_\perp,\omega) = -(k_\parallel^2+k_\perp^2)\Phi_{2,n}(k_\parallel,k_\perp,\omega) + aB_n(k_\perp)J_n(k_\perp a)\Phi'_{2,n}(k_\parallel,a,\omega), \quad \text{(A7)}$$

where we have used the second Green's identity and the Laplacian in cylindrical coordinates; here $\Phi_{2,n}(k_\parallel,k_\perp,\omega)$ is the inverse of (A3) [see (A2)],

$$\Phi_{2,n}(k_\parallel,k_\perp,\omega) = \frac{1}{(2\pi)^2}B_n(k_\perp)\int d^3r\,\Phi_2(\mathbf{r},\omega)J_n(k_\perp\rho)e^{-in\varphi}e^{-ik_\parallel z} \quad \text{(A8)}$$

and

$$\Phi'_{2,n}(k_\parallel,a,\omega) = \frac{1}{(2\pi)^2}\int_0^{2\pi} d\varphi\int_{-\infty}^{\infty} dz\left(\frac{\partial\Phi_2}{\partial\rho}\right)_{\rho=a} e^{-in\varphi}e^{-ik_\parallel z}. \quad \text{(A9)}$$

Combining (A6) and (A7), we obtain

$$\sum_{k'_\perp} E_n(k_\parallel,k_\perp,k'_\perp,\omega)\Phi_{2,n}(k_\parallel,k'_\perp,\omega) = aB_n(k_\perp)J_n(k_\perp a)\Phi'_{2,n}(k_\parallel,a,\omega) \quad \text{(A10)}$$

after introducing the quantity $E_n(k_\parallel,k_\perp,k'_\perp,\omega) = (k_\parallel^2 + k_\perp^2)\delta_{k'_\perp,k_\perp} - 4\pi\chi_n(k_\perp,k'_\perp,\omega)$ [24,33].

The expression (A10) allows us to obtain $\Phi_{2,n}(k_\parallel,k'_\perp,\omega)$ and rewrite the self-consistent potential inside the cylinder [Eq. (A3)] in the form

$$\Phi_2(\mathbf{r},\omega) = \sum_{n=-\infty}^{\infty}\int_{-\infty}^{\infty} dk_\parallel F_n(k_\parallel,\rho,\omega)\Phi'_{2,n}(k_\parallel,a,\omega)e^{in\varphi}e^{ik_\parallel z}. \quad \text{(A11)}$$

Writing $\Phi'_{2,n}(k_\parallel,a,\omega) \equiv A(k_\parallel,\mathbf{r}')b_n(k_\parallel)$, the expression (3) is recovered.

APPENDIX B: EVALUATION OF THE FUNCTION $F_n(k_\parallel,\rho,\omega)$

The factor $[k^2\epsilon(\mathbf{k},\omega)]^{-1}$ in (7) can be written as the sum of two contributions

$$\frac{1}{k^2\epsilon(\mathbf{k},\omega)} = \left(\frac{Q^2}{Q^2-Q_p^2}\right)\frac{1}{k^2} - \left(\frac{Q_p^2}{Q^2-Q_p^2}\right)\frac{1}{k^2-\left(Q^2-Q_p^2\right)},$$

where $Q^2 = \omega(\omega+i\gamma)/\beta^2$ and $Q_p^2 = \omega_p^2/\beta^2$. The function $F_n(k_\parallel,\rho,\omega)$ becomes

$$\begin{aligned} F_n(k_\parallel,\rho,\omega) &= a\left(\frac{Q^2}{Q^2-Q_p^2}\right)\sum_{k_\perp} B_n(k_\perp)J_n(k_\perp\rho)f_{1,n}(\mathbf{k},\omega) \\ &\quad - a\left(\frac{Q_p^2}{Q^2-Q_p^2}\right)\sum_{k_\perp} B_n(k_\perp)J_n(k_\perp\rho)f_{2,n}(\mathbf{k},\omega) \\ &\equiv \frac{a}{\epsilon_2(\omega)}f_{1,n}(k_\parallel,\rho,\omega) \\ &\quad + \frac{a}{\epsilon_2(\omega)}[\epsilon_2(\omega)-1]f_{2,n}(k_\parallel,\rho,\omega), \end{aligned} \quad \text{(B1)}$$

where

$$f_{1,n}(\mathbf{k},\omega) = \frac{B_n(k_\perp)J_n(k_\perp a)}{k_\parallel^2+k_\perp^2}, \quad f_{2,n}(\mathbf{k},\omega) = \frac{B_n(k_\perp)J_n(k_\perp a)}{\kappa^2+k_\perp^2},$$

with $\kappa^2 = k_\parallel^2 - (Q^2-Q_p^2)$ and $\epsilon_2(\omega) = 1 - Q_p^2/Q^2$. For a given value of $k_\parallel$, there is a $(k_\perp-\rho)$-transformation relation between $f_{i,n}(k_\parallel,k_\perp,\omega)$ and $f_{i,n}(k_\parallel,\rho,\omega)$,

$$f_{i,n}(k_\parallel,k_\perp,\omega) = B_n(k_\perp)\int_0^a d\rho\,\rho J_n(k_\perp\rho)f_{i,n}(k_\parallel,\rho,\omega), \quad i = 1,2.$$

Thus,

$$\frac{J_n(k_\perp a)}{p_i^2+k_\perp^2}=\int_0^a d\rho\,\rho J_n(k_\perp\rho)f_{i,n}(\rho,k_\parallel,\omega), \tag{B2}$$

with $p_1=k_\parallel$ and $p_2=\kappa$. To find $f_{i,n}(k_\parallel,\rho,\omega)$ we use the integral

$$\int d\rho\,\rho J_n(k_\perp\rho)I_n(p_i\rho) = \frac{p_i\rho J_n(k_\perp\rho)I_n'(p_i\rho)-k_\perp\rho I_n(p_i\rho)J_n'(k_\perp\rho)}{p_i^2+k_\perp^2}.$$

Using the fact that $k_\perp$ is such that $[J_n'(k_\perp\rho)]_{\rho=a}=0$ holds,

$$\int_0^a d\rho\,\rho J_n(k_\perp\rho)\left(\frac{I_n(p_i\rho)}{p_i a I_n'(p_i a)}\right)=\frac{J_n(k_\perp a)}{p_i^2+k_\perp^2}.$$

Therefore, according to (B2),

$$f_{i,n}(k_\parallel,\rho,\omega)=\frac{I_n(p_i\rho)}{p_i a I_n'(p_i a)},$$

which through (B1) leads to the expression (9).

[1] P. Halevi and R. Fuchs, in *Spatial Dispersion in Solids and Plasmas*, edited by P. Halevi (Elsevier, Amsterdam, 1992).

[2] A. Liebsch, *Electronic Excitations at Metal Surfaces* (Springer, Berlin, 1997).

[3] N. A. Mortensen, S. Raza, M. Wubs, T. Søndergaard, and S. I. Bozhevolnyi, Nat. Commun. **5**, 3809 (2014).

[4] S. Raza, M. Wubs, S. Bozhevolnyi, and N. A. Mortensen, Opt. Lett. **40**, 839 (2015).

[5] S. Raza, G. Toscano, A.-P. Jauho, M. Wubs, and N. A. Mortensen, Phys. Rev. B **84**, 121412(R) (2011).

[6] R. Filter, C. Bösel, G. Toscano, F. Lederer, and C. Rockstuhl, Opt. Lett. **39**, 6118 (2014).

[7] F. J. García de Abajo, J. Phys. Chem. **112**, 17983 (2008).

[8] J. M. McMahon, S. K. Gray, and G. C. Shatz, Nano Lett. **10**, 3473 (2010).

[9] A. I. Fernández-Domínguez, A. Wiener, F. J. García-Vidal, S. A. Maier, and J. B. Pendry, Phys. Rev. Lett. **108**, 106802 (2012).

[10] C. David and F. J. García de Abajo, ACS Nano **8**, 9558 (2014).

[11] Y. Luo, A. I. Fernández-Domínguez, A. Wiener, S. A. Maier, and J. B. Pendry, Phys. Rev. Lett. **111**, 093901 (2013).

[12] C. Ciraci, J. B. Pendry, and D. R. Smith, Chem. Phys. Chem. **14**, 1109 (2013).

[13] J. M. McMahon, S. K. Gray, and G. C. Schatz, Phys. Rev. Lett. **103**, 097403 (2009); Phys. Rev. B **82**, 035423 (2010).

[14] G. Toscano, S. Raza, W. Yan, C. Jeppesen, S. Xiao, M. Wubs, A.-P. Jauho, S. Bozhevolnyi, and N. A. Mortensen, Nanophotonics **2**, 161 (2013).

[15] A. V. Zayats and I. I. Smolyaninov, J. Opt. A **5**, S16 (2003).

[16] D. E. Chang, A. S. Sørensen, P. R. Hemmer, and M. D. Lukin, Phys. Rev. Lett. **97**, 053002 (2006).

[17] D. E. Chang, A. S. Sørensen, P. R. Hemmer, and M. D. Lukin, Phys. Rev. B **76**, 035420 (2007).

[18] A. V. Akimov, A. Mukherjee, C. L. Yu, D. E. Chang, A. S. Zibrov, P. R. Hemmer, H. Park, and M. D. Lukin, Nature (London) **450**, 402 (2007).

[19] M. Pelton, Nat. Photon. **9**, 427 (2015).

[20] M. S. Tame, K. R. McEnery, S. K. Özdemir, J. Lee, S. A. Maier, and M. S. Kim, Nat. Phys. **9**, 329 (2013).

[21] C. Tserkezis, N. Stefanou, M. Wubs, and N. A. Mortensen, Nanoscale **8**, 17532 (2016).

[22] H. Y. Xie, H. Y. Chung, P. T. Leung, and D. P. Tsai, Phys. Rev. B **80**, 155448 (2009).

[23] T. Christensen, W. Yan, S. Raza, A.-P. Jauho, N. A. Mortensen, and M. Wubs, ACS Nano **8**, 1745 (2014).

[24] C. Girard and F. Hache, Chem. Phys. **118**, 249 (1987).

[25] F. Hache, D. Ricard, and C. Girard, Phys. Rev. B **38**, 7990 (1988).

[26] M. Boustimi, J. Baudon, P. Candori, and J. Robert, Phys. Rev. B **65**, 155402 (2002).

[27] F. Forstmann and R. R. Gerhardts, *Metal Optics Near the Plasma Frequency* (Springer, Berlin, 1986).

[28] V. V. Klimov and M. Ducloy, Phys. Rev. A **69**, 013812 (2004).

[29] M. Boustimi, J. Baudon, and J. Robert, Opt. Commun. **198**, 389 (2001).

[30] I. Villó-Pérez and N. R. Arista, Surf. Sci. **603**, 1 (2009).

[31] L. Novotny, Appl. Phys. Lett. **69**, 3806 (1996).

[32] J. D. Jackson, in *Classical Electrodynamics*, 2nd ed. (Wiley, New York, 1975), pp. 106–107.

[33] D. M. Newns, Phys. Rev. B **1**, 3304 (1970).